International Forum on Aeroelasticity and Structural Dynamics
IFASD 2017
25-28 June 2017, Como - Italy

AEROELASTIC LIMIT CYCLE OSCILLATIONS ON A 3D WING

Sylvie Dequand[1], Guy-Daniel Mortchéléwicz[1], and Anne-Sophie Sens[2]

[1] Département Aérodynamique, Aéroélasticité, Acoustique
ONERA, The French Aerospace Lab
Sylvie.Dequand@onera.fr

[2] Département Réseau, Ingénierie et Maquettes
ONERA, The French Aerospace Lab
Anne-Sophie.Sens@onera.fr

Keywords: Aeroelasticity, LCO, Dynamic Coupled Simulations, Reduced Model.

Abstract: This contribution deals with Limit Cycle Oscillations (LCO), which are sustained periodic oscillations due to nonlinearities. The study has been carried out in close collaboration between DLR and ONERA, in the framework of the High Fidelity Aeroelastic Simulation (HIFAS) project. The investigations are related to the prediction of 3D LCO on the flexible "Aerostabil" backward-swept wing. For this 3D configuration, the DLR has experimentally simulated LCO in the TWG wind tunnel in Göttingen and has also numerically predicted it using CFD-CSM coupled simulations. We present the results obtained with the elsA code developed at ONERA for these experimental cases. The study of the nonlinear behavior of the first harmonic of the generalized aeroelastic forces (GAF) as a function of the amplitude shows the existence of a mode for which the aeroelastic force goes from stable to unstable. Through dynamic fluid-structure coupling computations on this mode, with the fluid modeled by averaged Navier Stokes equations and the Menter k-omega turbulence model, we find the existence of limit cycle oscillations. A nonlinear reduced model of the aeroelastic force is then presented. This model is constructed from the results obtained for the first harmonic of the aeroelastic forces computed by forced excitation simulating different frequencies and different excitation amplitudes. Comparisons between the fluid calculations and the dynamic coupling simulation using the nonlinear reduced model aeroelastic forces are presented. The occurrence of LCO is also investigated for the NLR 7301 two-dimensional airfoil. As for the 3D Aerostabil wing, a nonlinear reduced model for the first harmonic of the GAF is built. The fluid-structure simulations performed with this model confirms the existence of LCO and the capability of predicting the LCO phenomenon with a single DOF system.

1 INTRODUCTION

In this article, we are interested in Limit Cycle Oscillations (LCO), which are sustained periodic oscillations due here to fluid nonlinearities, the structure itself being considered linear. LCO have been a chronic problem on various combat aircrafts. We can mention, in particular, the work on the F16 [1].
In the years 2001/2002, the DLR investigated experimentally a flexible wing [2], called "Aerostabil", in the TWG wind tunnel in Göttingen. LCO have been obtained in the wind tunnel operation domain. Fluid-structure coupling simulations enabling LCO to be found were carried out with the TAU code [3]. Various turbulence models were tested and LCO were

obtained using the Menter k-ω model. To obtain these LCO numerically, the boundary layers of the side walls, floor and ceiling had to be introduced. Given that the TWG wind tunnel has adjustable high and low walls, the shape of these walls was also taken into account. The DLR showed that LCO could be simulated numerically only with the first mode (first bending).
In the context of the collaboration with the DLR on the HIFAS project, aeroelastic simulations were conducted at ONERA on this LCO problem with the elsA code [4], using averaged Navier Stokes equations associated with the Menter k-ω turbulence model. In a first section we present the results obtained with the elsA code and in a second section we present the construction of a nonlinear reduced model and the simulation of the LCO with this model.
In a third section we analyze the occurrence of LCO in the case of the NLR 7301 two-dimensional airfoil. We show that the LCO can be simulated numerically with only one mode.

2 LCO SIMULATION

In order to evaluate the numerical tools used for non-linear aeroelastic simulations and to study in close collaboration interesting aeroelastic phenomena, the case of the Aerostabil wing has been investigated both by DLR and ONERA.
Fluid-structure coupling simulations carried out by the DLR with the TAU code enabled to predict LCO [3] and to obtain a good agreement between experimental and numerical results (Figure 1). A mapping of the shutdown total pressure and Mach number was also performed, to reveal the areas in which LCO occurred (Figure 2).

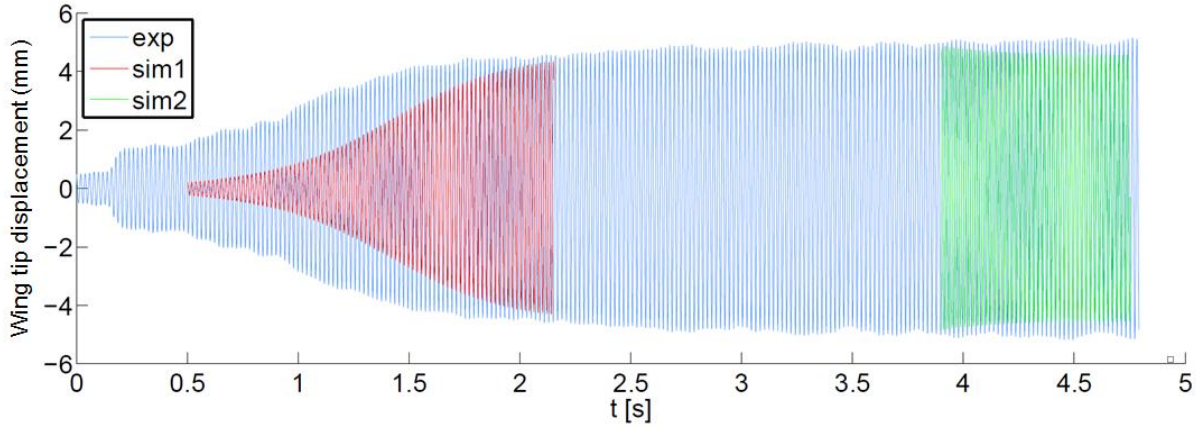

Figure 1: Time evolution of the wing tip displacement – Comparison between experimental and numerical solutions obtained by the DLR.

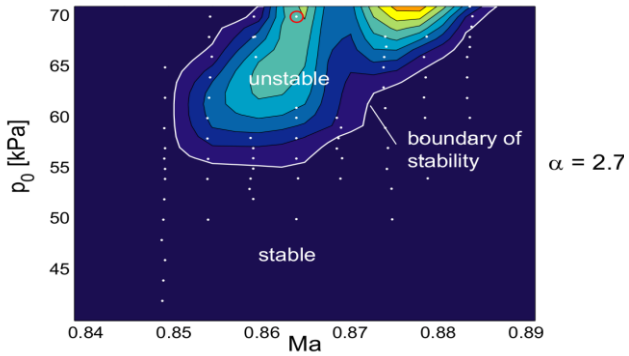

Figure 2: Stable and unstable areas of the Aerostabil wing in respect of Mach number and shutdown total pressure, at an angle of attack of 2.7°.

On ONERA side, computations have been performed with the CFD code elsA [4].

The LCO case discussed is defined by the following conditions: a Mach number of 0.865, incidence of 2.69°, upstream stagnation total pressure of 64428.8 Pa, and stagnation total temperature of 311.5 K. The Mach number is used to set the counter-pressure to be imposed downstream, as well as the initial field.
The Aerostabil wing has a wingspan of 0.610 m, a wing sweep angle of 32 degrees, and a chord of 0.2417 m at the root and of 0.0991m at the tip of the wing. The wing CAD is given as an IGES file describing the jig shape. The incidence is taken into account by rotating the wing about an axis transverse to the wind tunnel. A structured mesh of about 5 million cells has been built using the ICEM software and the wing and wind tunnel wall meshes were generated by creating O-blocks around these surfaces. The boundary layer mesh is obtained by refining it in the direction of the thickness. The mesh produced therefore includes the modelling of the boundary layers of the floor, ceiling and vertical walls of the tunnel. The shapes of the upper and lower walls (Figure 3) of the TWG wind tunnel are also introduced into the mesh.

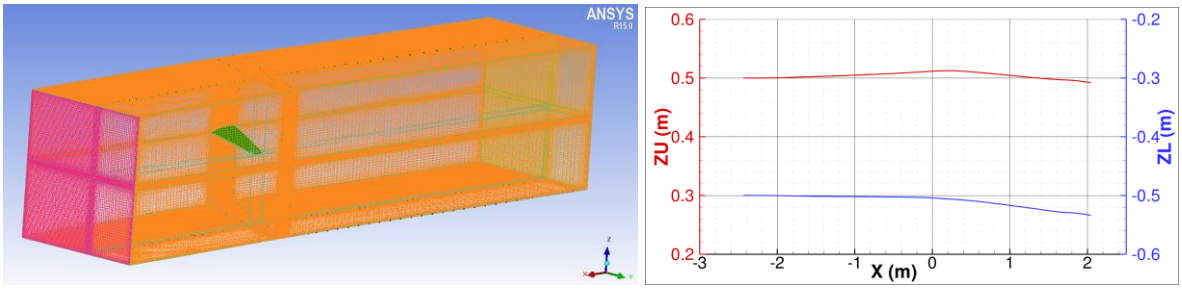

Figure 3: Mesh around the Aerostabil wing (left) and wind tunnel ceiling (ZU) and floor (ZL) shapes (right).

This mesh provides the correct stationary pressure field up to the wing root, as shown by the good agreement with the DLR results presented in Figure 4.

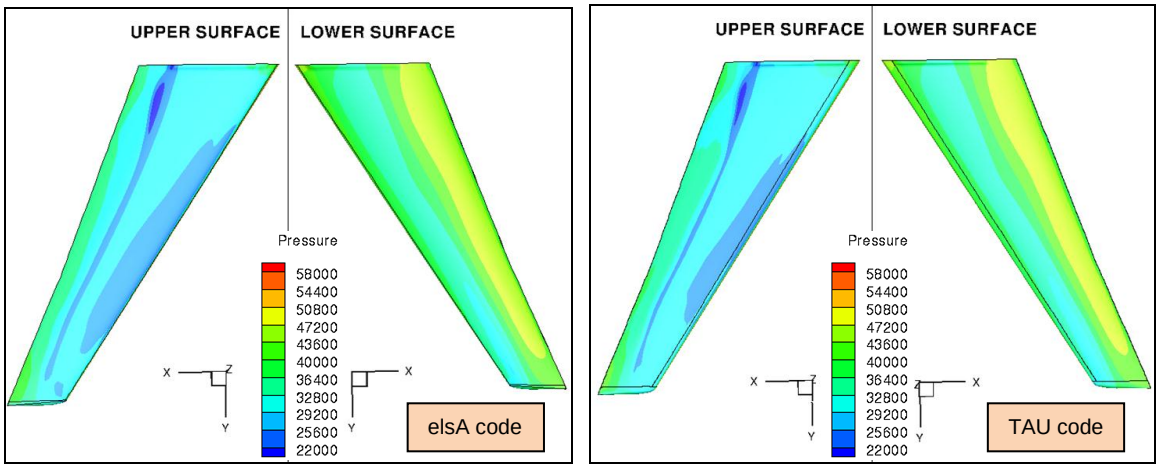

Figure 4: Stationary pressure distribution from CFD computations: elsA - ONERA code (left hand-side) vs TAU - DLR code (right hand-side).

The aeroelastic subsystem of the elsA code enables high-fidelity fluid-structure coupling simulations, ranging from non-linear and linearized harmonic forced motion computations, to static and dynamic coupling simulations in the time-domain with different structural approaches.
During fluid-structure coupling simulations, the flow and the structure computations are run separately, and a coupled solution is obtained by exchanging information at the fluid-structure interface. Thus, the fluid-structure coupling methodology consists in different steps:

- the flow solution is first computed over a given number of time steps,
- the aerodynamic loads are then computed at the center of each wall cell interface and transformed into an equivalent field on the structural nodes, ensuring a global conservation of forces and moments on the two grids,
- the mechanical equations are solved using either a reduced flexibility matrix of the structure or a modal approach,
- the structural displacements are transferred back onto the aerodynamic surface mesh using interpolation/fitting techniques,
- the aerodynamic mesh is finally deformed and updated. Two mesh deformation techniques are available in elsA. One is based on a structural linear analogy, and the second one is based on a mixed analytical/transfinite interpolation technique.

These steps are repeated until convergence of both flow and structural solutions.

In order to take into account the structural flexibility, the DLR has provided us with a modal base containing the first 10 flexible modes. Since this base is insufficient to represent the static deformations, we introduce the static shape calculated by the DLR (Figure 5). The latter was deduced from the numerical result obtained by the DLR, taking into account the true structural model. A set of 1000 points distributed over the wing lower and upper surfaces was extracted. Smoothing was carried out with the infinite volume method (generalization of the infinite plate method). These points were projected on the non-deformed wing. The displacement along the z direction corresponds to the static deformation to be introduced and static fluid-structure coupling simulations can then be performed.

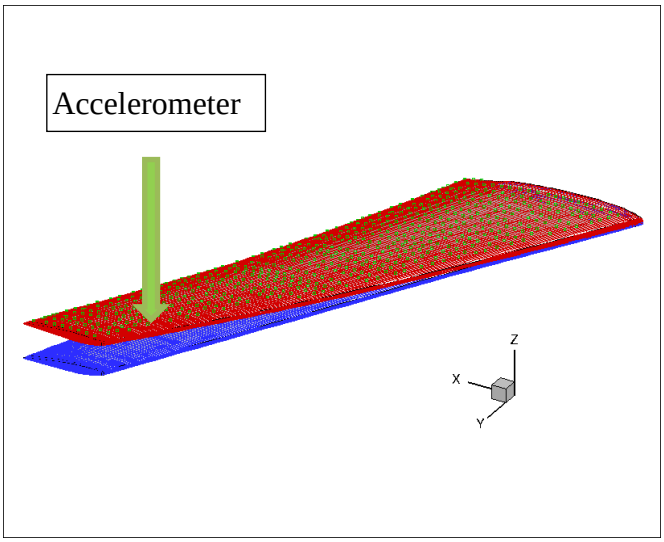

Figure 5: Smoothing of the static deformation calculated by the DLR with the TAU code.

Figure 6 shows the very good agreement between the deformed wing obtained with the elsA code and the TAU code for three different sections along the wing span. The comparison of the pressure evolution on the three sections shows also a good agreement except for the part related to the trailing edge where intermediate shocks are obtained.

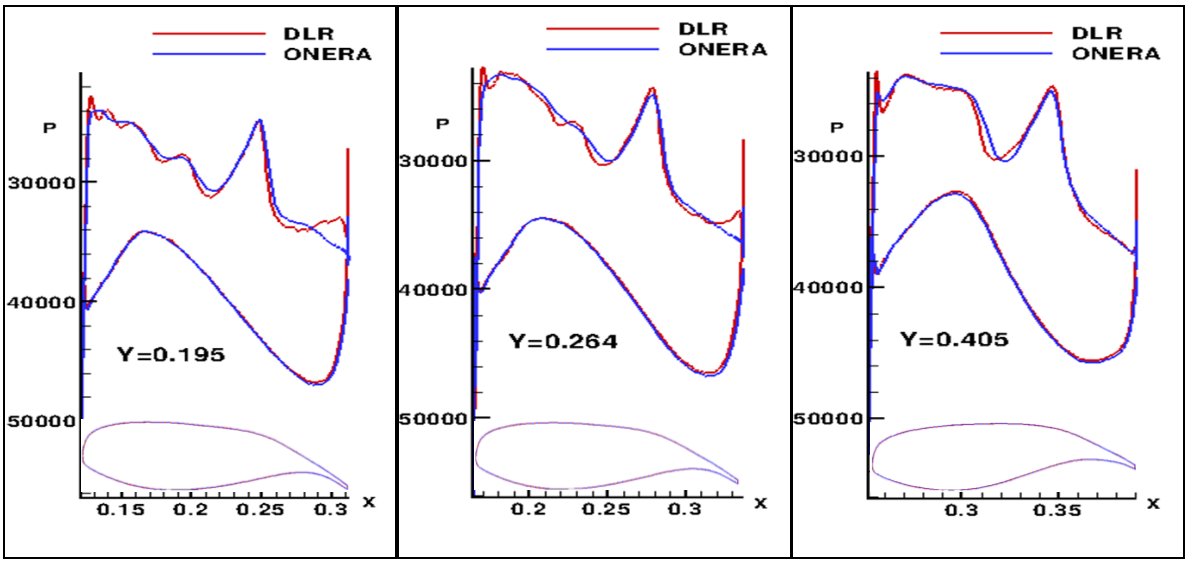

Figure 6: Static fluid-structure coupling simulations: comparison between the pressure distributions on three sections along the wing span, obtained by the TAU - DLR code, and by the elsA - ONERA code. The deformed wing is also shown for each section.

A dynamic calculation is performed taking into account the first bending mode of the wing (Figure 7) and using the dual time step method. At each time step, a stationary problem is solved at the time (n+1)Δt using a pseudo-unsteady method. The implicit phase takes into account the time term in (3 ΔW)/(2 Δt). This allows a CFL number of 10^{10} to be used achieving convergence at each time step of the relative residuals. This property remains true as long as the airflows are not too much separated. The time sizing of the calculation has been set in order to obtain four seconds of physical time. The LCO frequency being around 50 Hz, 200 periods are simulated with 64 time steps per period. At each time step, 2 structural iterations are performed. With the sizing used to calibrate the structural modes and structural matrices, the initial condition is defined by $\dot{q}(0) = 37$.

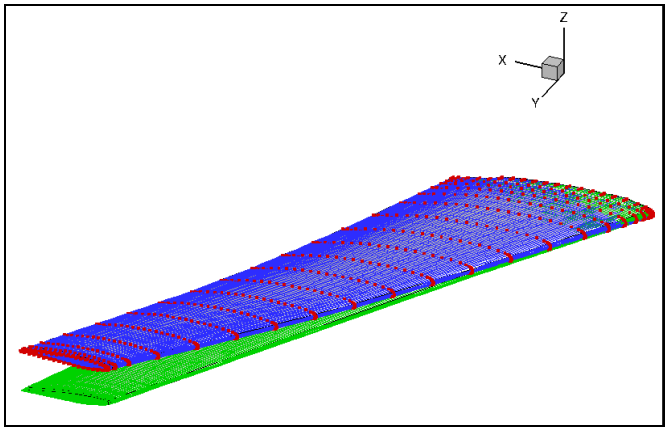

Figure 7: First bending mode of the Aerostabil wing.

In Figure 8, we show the displacement obtained by the accelerometer as positioned in Figure 5. The Prony analysis of the displacement calculated at this sensor gives a frequency of 51.34 Hz and an amplitude of 5 mm. This result is very similar to the experimental data obtained for which a displacement of 5 mm and a frequency of 47 Hz were observed.

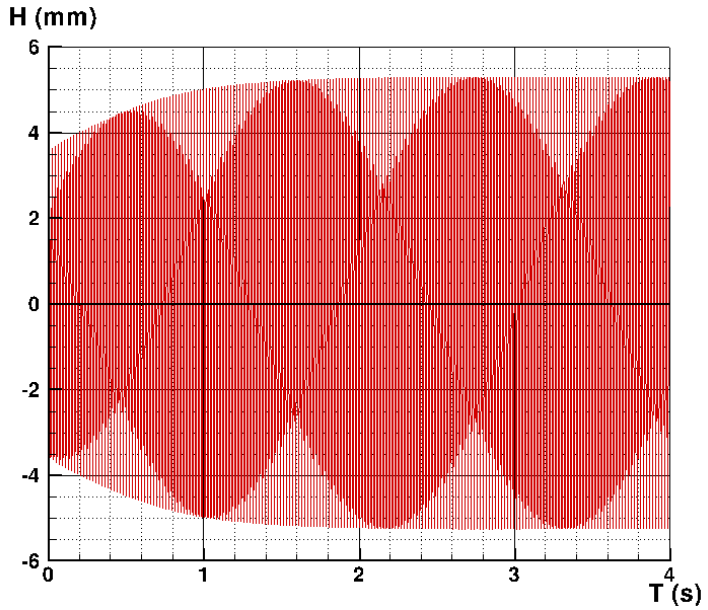

Figure 8: LCO obtained with the elsA code for the initial condition $\dot{q}(t=0)=37$.

A new dynamic coupling calculation is performed over 1 second with the initial condition $\dot{q}(0)=80$. This means that, at the start of the simulation, the amplitude is greater than that of the limit cycle. The generalized coordinate decreases to stabilize and to converge toward the amplitude of the limit cycle (Figure 9).

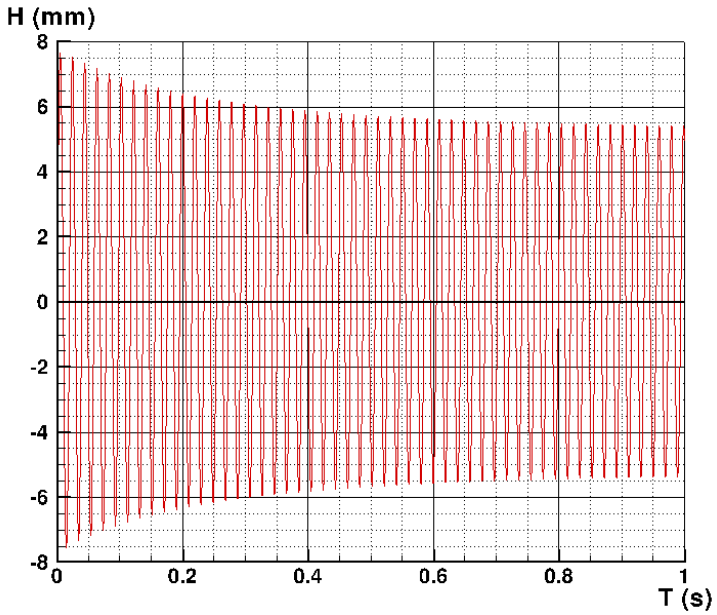

Figure 9: LCO obtained with the elsA code for the initial condition $\dot{q}(t=0)=80$.

In Figure 10, a visualization of the pressure field evolution for the section y = 0.478 m (corresponding to the ordinate position of the sensor) shows the presence of two shocks. The upstream shock disappears to blend with the second and then reforms. The LCO phenomenon is due to this particular behavior.

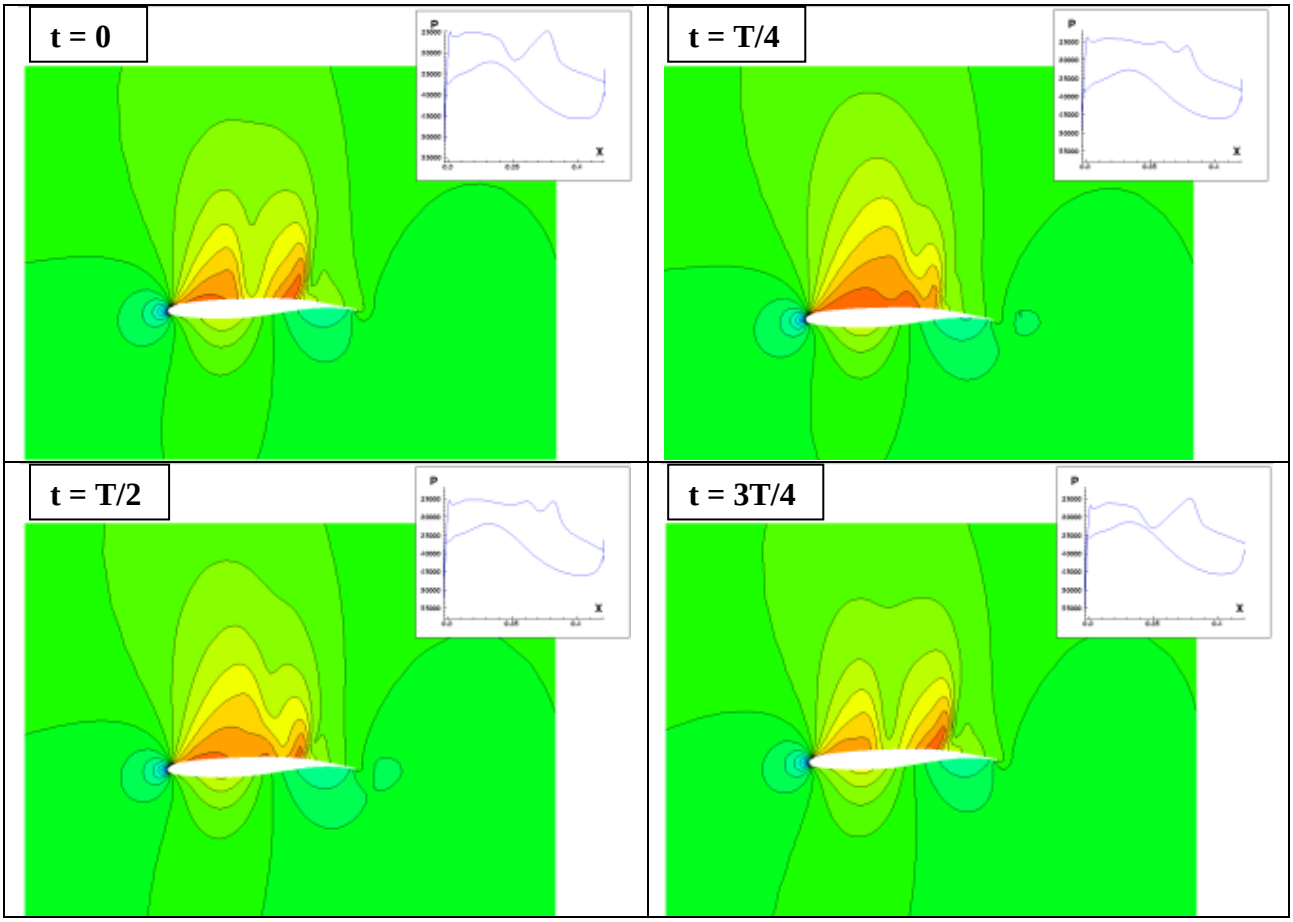

Figure 10: Evolution of the pressure field, calculated with the elsA code on a cycle for the section y = 0.478.

The pressure field shocks observed in Figure 10 can be explained by calculating the generalized aerodynamic force (GAF) of the system. The first harmonic of the GAF is expressed as:

$$GAF = \frac{1}{\frac{1}{2}\rho_\infty V_\infty^2} \int p_1 \, n.\phi \, d\sigma \quad GAF = \frac{1}{\frac{1}{2}\rho_\infty V_\infty^2} \int p_1 n \cdot \phi \quad d\sigma \tag{1}$$

where p_1 is the first harmonic of the pressure (complex number), n is the normal, and ϕ is the first mode. The imaginary part of the GAF density (D) shown in Figure 11 is written as:

$$D = \mathrm{Im}(p_1) \quad n \cdot \phi \tag{2}$$

The stable zones are defined by D> 0 and unstable areas are defined by D <0. It is mainly the area at the end of the wing upper surface that is unstable.

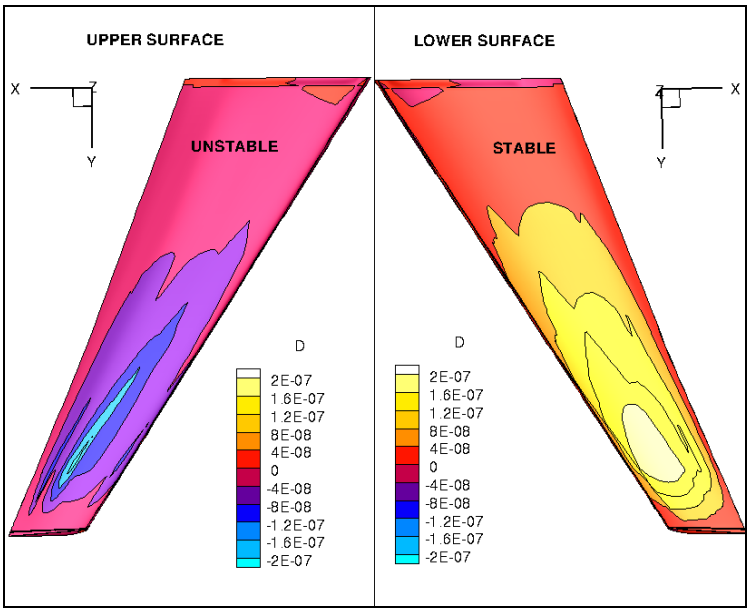

Figure 11: Imaginary part of the density D of the GAF obtained with the elsA code.

The results presented in this section show that dynamic fluid-structure coupling simulations carried out with the elsA code are able to predict the LCO phenomenon observed experimentally on the Aerostabil wing.
In the next section, a reduced model of the GAF is built and its ability of predicting LCO is investigated.

3 REDUCED MODEL

Given that the structure is linear, the occurrence of LCO can only be due to non-linearities associated with aerodynamic forces. Aeroelastic phenomena are usually linked to the first pressure harmonic and we can show that the first harmonic of the GAF, obtained by simulating a harmonic forced movement of the first mode, depends non-linearly on the amplitude. The GAF are thus calculated by simulating a harmonic forced excitation of the first mode for the 10 Hz, 20 Hz, 30 Hz, 40 Hz, 50 Hz, 60 Hz, 70 Hz, and 80 Hz frequencies and for amplitudes of 0.01, 0.05, 0.10, 0.15 and 0.20. Each simulation is carried out over 5 periods. The evolution of the first harmonic of the GAF is shown Figure 12. The dependence of the GAF on the amplitude is low but observable. At a frequency of 50 Hz, corresponding to the LCO frequency, the solution is unstable for small amplitudes and it becomes stable for larger amplitudes.
The study of the mechanical system stability for fluid-structure coupling with 1 degree of freedom boils down to studying the sign of the imaginary part of the GAF. If it is positive, the system is stable; if it is negative, the system is unstable (this result is obtained by writing the aerodynamic forces on the left side of the structural dynamics equations). The change in stability occurs around the frequency of 50 Hz. For this wing, this sign change criterion gives us the means to predict the limit cycles.
The limit cycle would be explained as follows: for low-amplitudes motion is unstable and tends to become amplified. Once it reaches a sufficient enough amplitude it becomes stable and tends to undergo a damped motion.

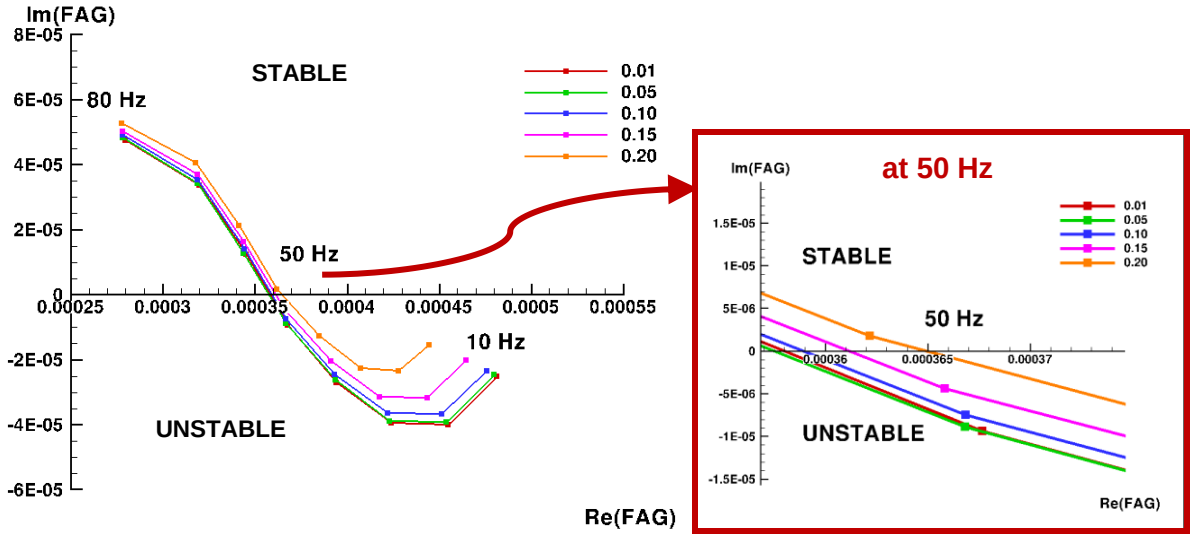

Figure 12 : GAF calculated by simulating a harmonic forced excitation of the first mode for the 10Hz, 20Hz, 30Hz, 40Hz, 50Hz, 60Hz, 70Hz, and 80Hz frequencies and for amplitudes of 0.01, 0.05, 0.10, 0.15 and 0.20.

The methodology for building the reduced model is based on a nonlinear variant of the Roger model [5], already presented in 2011 [6]. A state-space representation of the system is written and comprises P auxiliary equations, introducing P auxiliary variables η_i :

$$\begin{cases} \dfrac{1}{V_\infty^2}\ddot{\eta}_i - \dfrac{2\,p_i}{V_\infty}\dot{\eta}_i + \left(p_i^2 + \omega_i^2\right)\eta_i = q(t) \\ f = \overline{f} - \overline{f_s} = \displaystyle\sum_{i=1}^{P}\sum_{j=1}^{N_c} D_{ij}(\eta_i)^{2j-1} + \sum_{j=1}^{N_{D_0}} D_{0,j}(q_j)^{2j-1} + \sum_{j=1}^{N_{D_1}} D_{1,j}\left(\dfrac{\dot{q}_j}{V_\infty}\right)^{2j-1} + \sum_{j=1}^{N_{D_2}} D_{2,j}\left(\dfrac{\ddot{q}_j}{V_\infty^2}\right)^{2j-1} \end{cases} \tag{3}$$

where p_i and ω_i are the conjugated complex poles ($p_i \pm i\omega_i$) selected from the steady half-plane. The force f is the unsteady force applied to the airfoil and D_{ij}, $D_{0,j}$, $D_{1,j}$, $D_{2,j}$ are the real matrix coefficients of the model to be determined.

For a harmonic excitation of the type: $q(t) = q_0 \cos(\omega t)$ and introducing the reduced frequency $k = \omega / V_\infty$, it can be shown that the first harmonic of the generalized aeroelastic forces $F(k)$ is written in the frequency domain as:

$$F(k) = \sum_{j=1}^{N_C} H(j) \sum_{i=1}^{p} D_{ij} \left|\eta_i(k)\right|^{2(j-1)} \frac{1}{Z_i(k)} + \sum_{j=1}^{N_{D^0}} H(j) D_{0,j} q_0^{\,2(j-1)} + i \sum_{j=1}^{N_{D^1}} H(j) D_{1,j} k^{2j-1} q_0^{\,2(j-1)} + \sum_{j=1}^{N_{D^2}} H(j) D_{2,j} k^{2(2j-1)} q_0^{\,2(j-1)} \tag{4}$$

with :

$$Z_i(k) = p_i^2 + \omega_i^2 - k^2 - \underline{i}2\,p_i k$$

$$\eta_i(k) = \frac{q_0}{Z_i(k)} \tag{5}$$

$$H(j) = \frac{1}{2^{2(j-1)}} \frac{(2j-1)!}{(j-1)!\;\;(j)!}$$

and where the imaginary number $\underline{i}$ fulfills $\underline{i}^2 = -1$.
A random draw of the poles is performed for a given range of reduced frequency. For each draw, the model coefficients are obtained by solving a least square problem. For the Aerostabil wing, the GAF nonlinear reduced model is achieved by using $P = 4$, $N_C = N_{D_0} = N_{D_1} = N_{D_2} = 2$. As shown in Figure 13, the GAF obtained with this reduced model are in very good agreement with those calculated with the elsA code.

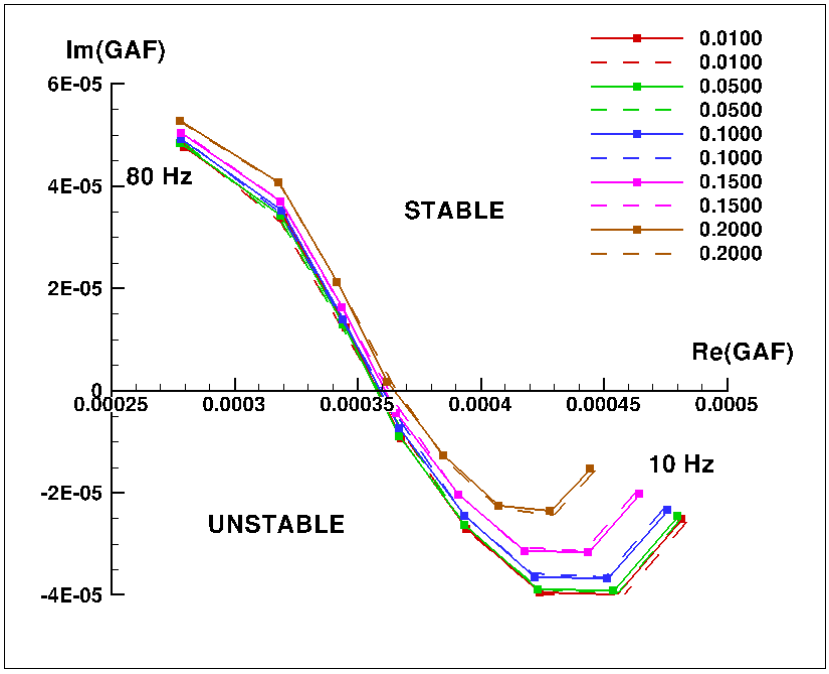

Figure 13: Comparison of the GAF obtained with the reduced model (dashed line) and those calculated with the elsA code (symbols).

This GAF nonlinear reduced model built can then be used to simulate fluid-structure interaction. The complete fluid-structure reduced model is then composed of the auxiliary equations and the GAF modelling equation of the system (3), to which the structural equations are added:

$$\underline{m}\ddot{q} + \underline{k}q + \frac{1}{2}\rho_\infty V_\infty^2 \left(\overline{f} - \overline{f_s}\right) = 0 \tag{7}$$

where the generalized mass and generalized stiffness of the mode are written as $\underline{m}$ and $\underline{k}$.
This complete system is re-written in matrix form:

$$\mathbf{M}\,\ddot{\mathbf{U}} + \mathbf{C}\,\dot{\mathbf{U}} + \mathbf{K}\mathbf{U} + \mathbf{F}\left(\mathbf{U}, \dot{\mathbf{U}}, \ddot{\mathbf{U}}\right) = \mathbf{0} \tag{8}$$

with:

$$\mathbf{U} = \begin{pmatrix} \eta \\ q \end{pmatrix}, \ \mathbf{F}\left(\mathbf{U}, \dot{\mathbf{U}}, \ddot{\mathbf{U}}\right) = \begin{pmatrix} 0 \\ \frac{1}{2}\rho_\infty V_\infty^2 \left(\overline{f} - \overline{f_s}\right) \end{pmatrix}$$

and: $\mathbf{M} = \begin{pmatrix} \frac{1}{V_\infty^2} I_d & 0 \\ 0 & \underline{m} \end{pmatrix}$, $\mathbf{C} = \begin{pmatrix} diag\left(-\frac{2\,p_i}{V_\infty}\right) & 0 \\ 0 & 0 \end{pmatrix}$, $\mathbf{K} = \begin{pmatrix} diag\left(p_i^2 + \omega_i^2\right) & -I_d \\ 0 & \underline{k} \end{pmatrix}$.

This equation is integrated using the Newmark scheme [7] with the constants $\gamma = 1/2$ and $\beta = 1/4$ which make it unconditionally stable and without numerical damping:

$$\begin{aligned} \dot{\mathbf{U}}_{t+\Delta t} &= \dot{\mathbf{U}}_t + \frac{\Delta t}{2}\left[\ddot{\mathbf{U}}_t + \ddot{\mathbf{U}}_{t+\Delta t}\right] \\ \mathbf{U}_{t+\Delta t} &= \mathbf{U}_t + \Delta t \dot{\mathbf{U}}_t + \frac{\Delta t^2}{4}\left[\ddot{\mathbf{U}}_t + \ddot{\mathbf{U}}_{t+\Delta t}\right] \end{aligned} \tag{9}$$

The nonlinear equation is solved by using a fixed-point iteration method. Convergence of the method is observed after 11 sub-iterations.

With the amplitude normalization selected for the first mode, the structural model is defined by the following constants for the first mode: $\underline{m} = 0.000196$, $\underline{k} = 12.6$. The dynamic coupling is simulated for the initial condition $\dot{q}(0) = 37$. A LCO is obtained (Figure 14) with an amplitude and frequency comparable to those obtained by direct simulation (Figure 8). The Prony analysis enables to determine a LCO frequency of 51 Hz.
A second simulation is performed with a stronger initial condition $\dot{q}(0) = 80$ and the results are shown in Figure 15. As for the direct numerical simulation shown in Figure 9, the amplitude decreases and converges towards the LCO amplitude.
For both initial conditions, the orbits shown in the phase diagrams of Figure 14 and Figure 15 are highly similar to those computed with the elsA code.

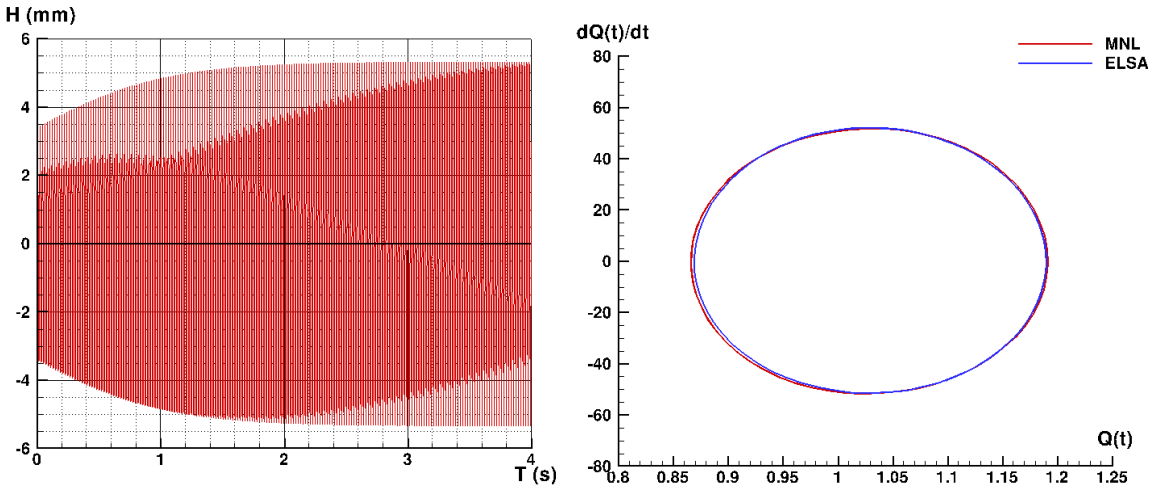

Figure 14 – LCO simulation with the nonlinear reduced model for the initial condition $\dot{q}(0) = 37$.
Phase diagram: elsA simulation (blue) vs nonlinear reduced model (red).

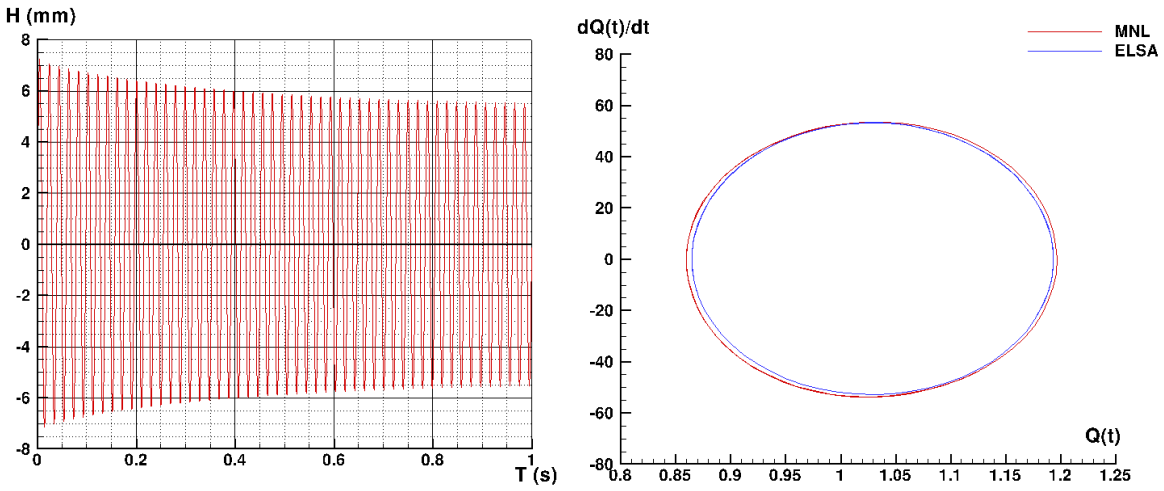

Figure 15 - LCO simulation with the nonlinear reduced model for the initial condition $\dot{q}(0) = 80$.
Phase diagram: elsA simulation (blue) vs nonlinear reduced model (red).

4 LCO FOR NLR 7301 AIRFOIL

A model to simulate the bi-dimensional flow around the NLR 7301 airfoil was developed at DLR [8]. The chord of the airfoil is 0.3 meter and the span 1 meter. A mechanical assembly, Figure 16, was used to simulate two degrees of freedom for the airfoil. The first is a vertical displacement, and the second a rotation about a transverse axis situated in the forward quarter of chord. The matrices for mass $\begin{pmatrix} m_h & -S_h \\ -S_h & I_{c/4} \end{pmatrix}$, damping $\begin{pmatrix} D_h & 0 \\ 0 & D_\alpha \end{pmatrix}$ and stiffness $\begin{pmatrix} K_h & 0 \\ 0 & K_\alpha \end{pmatrix}$ are defined by the following values:

m_h =25.93 kg, S_h = 0.377 kg m, $I_{c/4}$ = 0.091 kg m2, D_h = 78.23 kg s-1,
D_α = 0.202 kg m s-1 rad-1, K_h = 1.11 106 N m-1, K_α = 6.70 103 N m rad-1.

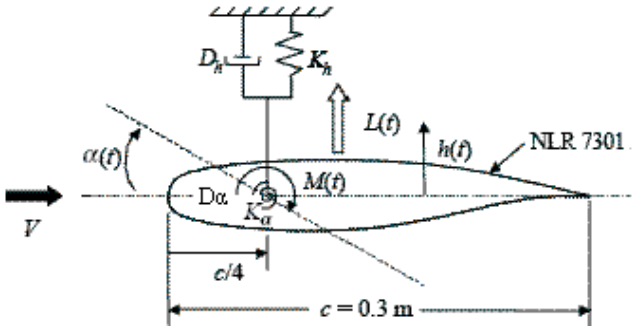

Figure 16 - Mechanical assembly for the NLR 7301 airfoil.

Aerodynamic limit cycles were observed for batch MP77 at the following aerodynamic conditions: upstream Mach number 0.754, stagnation pressure 45000 Pa, total temperature 309.7 K. The incidence is fixed at 0.5 degrees in order to obtain LCO.
The mechanical system is diagonalized and two structural modes are obtained, which are linear combinations of pumping and pitching. A multiplying coefficient of 0.01745 is applied so as to reduce the amplitude of these modes. The generalized masses and eigenfrequencies are, respectively, for each of the flexible modes, 0.000401 kg m ^{2} and 0.0000278 kg m ^{2}, 31.81 Hz and 46.11 Hz.
The fluid calculations are performed using the averaged Navier Stokes equations associated with the Menter k-ω turbulence model, on a multigrid structured mesh (with 2 levels of

subgrids) containing 24320 cells (Figure 17). For the aerodynamic conditions given above, a static coupling calculation is performed. A comparison between the stationary pressure field and the experimental result is shown in Figure 17.

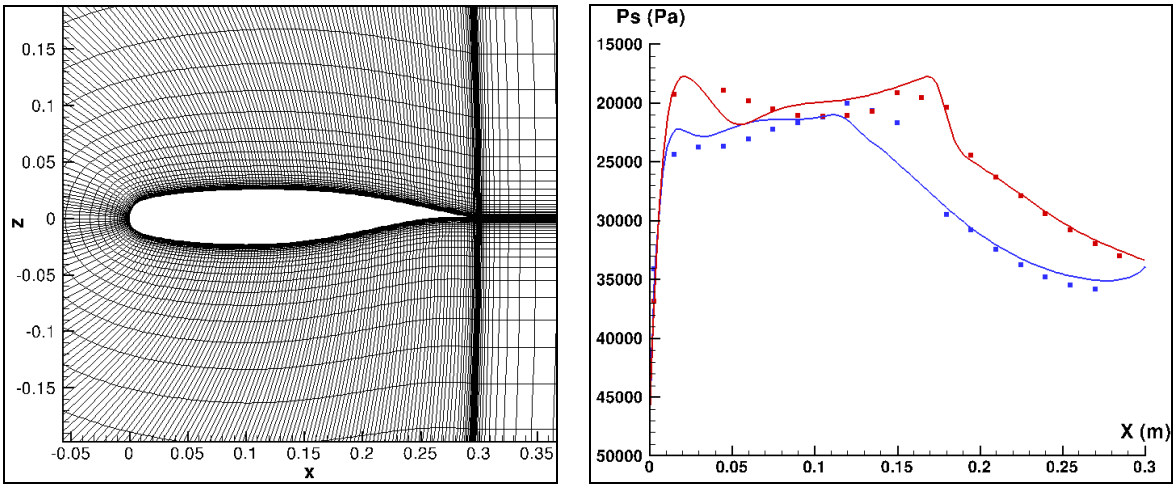

Figure 17 – Mesh around the supercritical NLR 7301 airfoil (left-hand side) and MP77 test case: pressure field on the airfoil (right-hand side).

Dynamic coupling simulations are performed for two initial conditions ($\dot{q}(0) = 200$ and $\dot{q}(0) = 275$). The sampling frequency is 6400 Hz and 6400 time steps are calculated, that is, a physical time of 1 s. The results in Figure 18 show that, for both initial conditions, LCO is obtained.

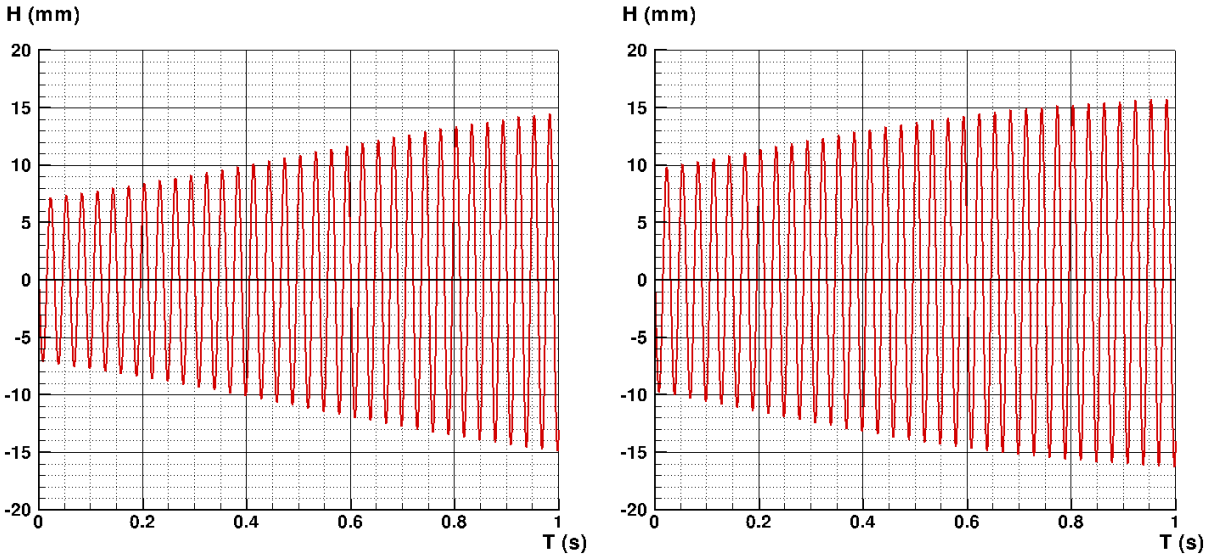

Figure 18 - Dynamic coupling obtained with the elsA code for initial conditions $\dot{q}(0) = 200$ and $\dot{q}(0) = 275$.

The GAF matrices are calculated for 8 frequencies from 10 Hz to 80 Hz and 5 magnitudes 0.1, 0.5, 1.0, 1.5, and 2.0. As in the case of the "Aerostabil" wing, the imaginary part of the term 1-1 of the GAF goes from stable to unstable for a frequency between 30 and 40 Hz (Figure 19), while the imaginary part of the term 2-2 remains stable ((Figure 20).

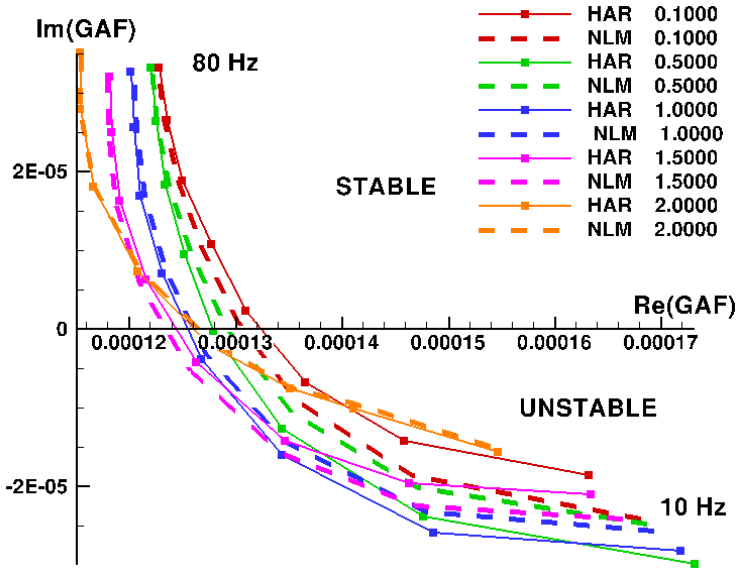

Figure 19 – Evolution of the term 1-1 of the GAF calculated with the elsA code (symbols); comparison with the nonlinear reduced model.

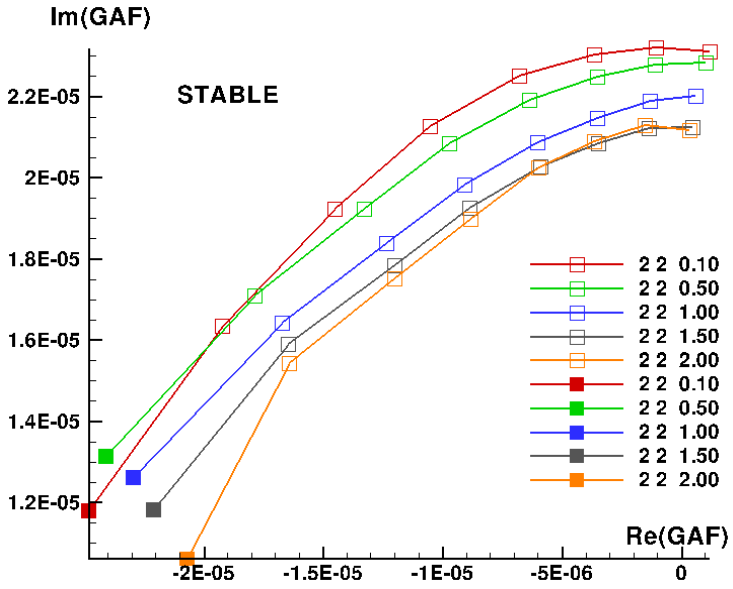

Figure 20 - Evolution of the term 2-2 of the GAF calculated with the elsA code.

A nonlinear reduced model for the term 1-1 of the GAF (Figure 19) is then built with the following parameters: $P = 7$, $N_C = 3$, and $N_{D_0} = N_{D_1} = N_{D_2} = 2$.

The fluid-structure coupling simulation performed with this model yields to the occurrence of limit cycles. Figure 21 and Figure 22 show the displacement of the airfoil trailing edge for two different initial conditions $\dot{q}(0) = 200$ and $\dot{q}(0) = 275$. On the right-hand side of these figures, the LCO orbits are compared with those obtained with the elsA code. Despite the introduction of a phase shift, the orbits remain highly similar.

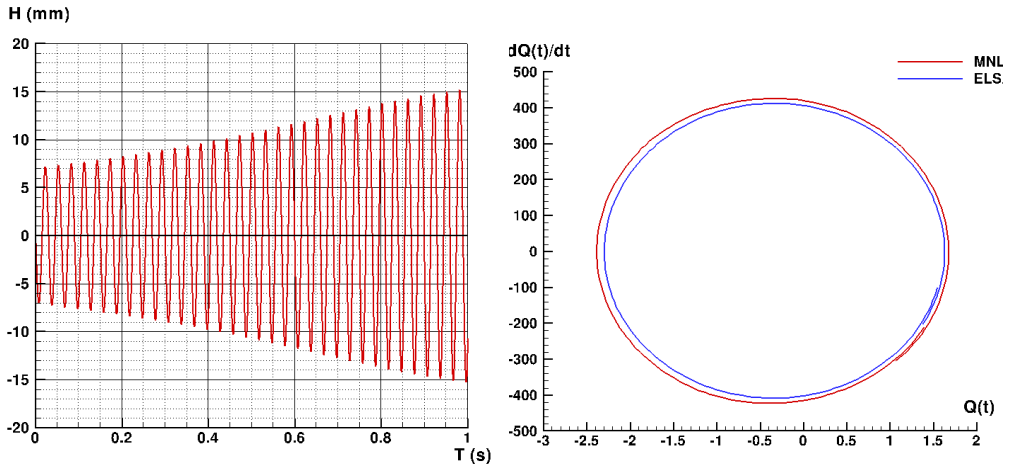

Figure 21 - LCO simulation obtained with the nonlinear reduced model for the condition $\dot{q}(0) = 200$.
Phase diagram: elsA simulation (blue) vs nonlinear reduced model (red).

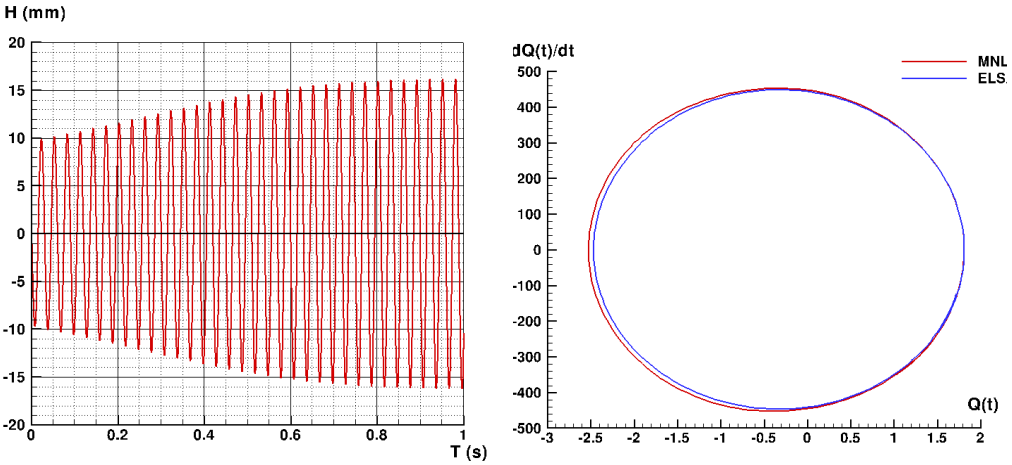

Figure 22 – LCO simulation with the nonlinear reduced model for the condition $\dot{q}(0) = 275$.
Phase diagram: elsA simulation (blue) vs nonlinear reduced model (red).

5 CONCLUSIONS

Dynamic fluid-structure coupling computations have been carried out on the Aerostabil wing in order to simulate limit cycle oscillations. The simulations are performed using the elsA code and enable to predict the LCO phenomenon investigated previously by the DLR, both experimentally and numerically. The occurrence of LCO is highly influenced by the mesh topology and a particular attention must be paid to the simulation of the boundary layers of the wind tunnel walls. Furthermore, the modal approach used in elsA for dynamic coupling computations requires a sufficient modal representation of the structure. However, the modal basis available was only composed of 10 structural modes and was insufficient to represent the static deformations. The dynamic simulations were therefore performed by deducing the static deformation to be introduced from the static numerical results obtained by the DLR. LCO was thus obtained taking into account the first bending mode of the wing but considering the complete structural model.
The study of the first harmonic of the generalized aeroelastic force due to a harmonic forced excitation for different excitation frequencies shows a dependence on the motion amplitude. A sign change of the imaginary part of the GAF is observed for frequencies in the vicinity of the LCO frequency. This important property may thus be used to check the possible occurrence of LCO phenomenon.

For the mode used to simulate the LCO, a nonlinear reduced model of the GAF was implemented using the first harmonic of the GAF obtained by harmonic forced excitation for different amplitudes and different frequencies. The simulation of the fluid-structure coupling with this model was used to simulate the LCO, in good agreement with results given by direct simulation in the time domain.

This methodology was finally applied to the two-dimensional flow around the NLR-7301 airfoil. The fluid-structure simulations performed with this model confirms the existence of LCO and the capability of predicting the LCO phenomenon with a single DOF system.

6 ACKNOWLEDGEMENTS

The authors would like to thank the *Deutsches Zentrum für Luft und Raumfahrt* for many discussions during the HIFAS project.

7 REFERENCES

[1] Bunton R. W. and Denegri, C.M. (2000). Limit cycle oscillation characteristics of fighter aircraft. *Journal of Aircraft*, 37(5), 916-918.

[2] Dietz G., Schewe G., KieBling F., Sinamiius M. (2003). Limit-cycle-oscillation experiments at a transport aircraft wing model. *International forum of aeroelasticity and structure dynamics (IFASD)*, Amsterdam, The Netherlands.

[3] Stickan B., Dillinger J., Schewe G. (2014). Computational aeroelastic investigation of a transonic limit-cycle-oscillation experiment at a transport aircraft wing model. *Journal of fluids and structures*, 49, 223-241.

[4] Cambier L., Heib S., Plot S. and Mayeur J. (2013). The Onera elsA CFD software: input from research and feedback from industry. *Mechanics & Industry*, 14(3), 159-174.

[5] Roger K. (1977). Airplane math modeling methods for active control design. *Structural Aspects of Active Controls, AGARD-CP-228*, 4, 1-11.

[6] Mortchéléwicz G. (2011). Application of the Levenberg Marquard algorithm to aeroelastic problems. *51st Israel annual conference on aerosce sciences*. Tel Aviv, Israel.

[7] Alarcon A. (2015). *Code Aster. Algorithmes d'intégration temporelle de l'opérateur DYNA_TRAN_MODAL.*

[8] Schewe G., Mai H., Dietz G. (2003). Nonlinear effects in transonic flutter with emphasis on manifestations of limit cycle oscillations. *Journal of fluids and structures*, 18(1), 3-22..

COPYRIGHT STATEMENT